Orbital
The electronic journal of chemistry

the electronic journal of chemistry

Full Paper | http://dx.doi.org/10.17807/orbital.v17i2.20255

Bactericidal and Bioactive Ceramic Scaffold

Camila Dias de Oliveira [a], Gabrieli Andressa de Campos [a], Juliana Cheleski Wiggers [a], Elvio A. de Campos [a], and Silvia Denofre de Campos* [a]

Infections caused by bacteria are among the main factors for the rejection of materials used in implants. Ceramic scaffolds containing silver have been shown to be bioactive and bactericidal for different strains of bacteria. In this work, glasses containing silver were synthesized by the sol-gel method to obtain scaffolds. Bands were observed in the 1200–930 cm^{-1} region that can be attributed to Si–O–Si bonds, but also bands of overlapping phosphate groups, bands at 490 cm^{-1} of Si–O–NBO, Si–O-Zn, and diffraction peaks corresponding to the hydroxyapatite phase. Bioactivity tests in the presence of the body fluid simulating solution (SBF) and antibacterial activity tests indicate that the glass and scaffolds are bioactive and bactericidal.

Graphical abstract

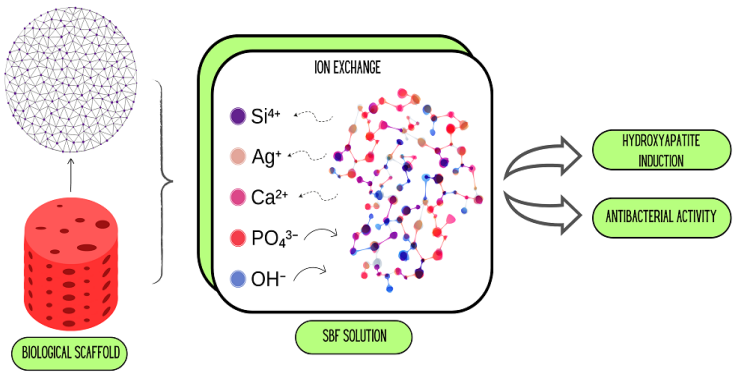

Keywords

Antibacterial
Bioglass scaffolds
Hydroxyapatite
Silver nanoparticle

Article history

Received 19 Feb 2024
Revised 21 Mar 2024
Accepted 20 Dec 2024
Available online 17 Apr 2025

Handling Editor: Sergio R. Lazaro

1. Introduction

To improve the quality of life of people who are victims of accidents or diseases that lead to the loss of living tissue, the use of implants that can replace injured parts of living tissue and restore their functions has become increasingly frequent. These materials are classified as biomaterials [1].

Biomaterials can be of synthetic or natural origin, solid or liquid, and used in the form of prostheses directly in contact with the biological system or as specific components in medical devices [1-2].

One of the biggest problems that doctors and patients face in the area of bone tissue reconstruction (orthopedic and dental) are infections caused by bacteria, especially after the surgical procedure, which may involve additional surgery, implant rejection, and even the death of the patient [3].

To treat these infections high doses of antibiotics are used, which are absorbed into the bloodstream. The problem observed in these cases is the increased resistance of some bacteria to these drugs, making it difficult to control the infection. Thus, the interest in biomaterials with antibacterial agent in their composition has become attractive as an implant, since the implanted material it also promotes *in loco* infection control [4].

Among the most used biomaterials for bone regeneration, hydroxyapatite is distinguished by promoting greater osteoconductivity and biocompatibility [5]. However, hydroxyapatite doesn't have antibacterial activity [4].

[a] Universidade Estadual do Oeste do Paraná, Rua da Faculdade, 645, Jardim La Salle, zip code 85903-000, Toledo, Paraná, Brazil.
*Corresponding author. E-mail: **silviadenofre@uol.br**

Silver nanoparticles (Ag) are widely studied due to their antibacterial properties and ease of being incorporated into the structure of glasses and ceramics in therapeutic concentrations ranging from 0.1 to 1.6 mg L^{-1}, eliminating bacteria without harming eukaryotic cells. Thus, for Ag^{+} ions to be properly incorporated into the vitreous lattice, it is necessary to have control over how they are released, starting with their stabilization [6].

From this perspective, tissue engineering proposes to work with scaffolds, which are three-dimensional structures with interconnected pores capable of releasing bacterial agents in a controlled manner. These pores also assist in the process of vascularization and cell proliferation, accelerating absorption and cell growth [7-8]. Glasses and ceramics with compositions based on SiO_2–P_2O_5–CaO systems have been highlighted in obtaining bioactive scaffolds, which can be obtained with different compositions [9]. It is known that the composition of these biomaterials and their method of obtaining directly influence their properties, such as bioactivity and degradability [6].

The sol-gel method is widely used in the synthesis of glasses of varied compositions that can be used to obtain scaffolds due to the ease in controlling properties, from nano to macro, obtaining a structure of easy expansion, and with the ability to include therapeutic or antibacterial agents [10]. This method has been used to manufacture scaffolds with a surface area greater than 100 m^2/g, with pore control, and good interconnectivity [11].

Of the techniques used to obtain scaffolds, salt leaching uses salt with soluble particles of handling, low cost, and porosity controlled by the granulometry of the salt used [11]. Another technique used is calcination, in which there is the formation of macro and micro porosity from the volatilization of organic materials. Calcination can affect the surface area, degradation rate, particle size, and crystalline phase of the material [12].

Thus, in this work, ceramic scaffolds were synthesized using salt leaching and polymeric calcination techniques based on glass-ceramics of composition $49SiO_2$-31CaO-$19P_2O_5$-$1Ag_2O$, obtained by the sol-gel method. The physicochemical properties of these scaffolds were analyzed by Fourier transform infrared spectroscopy (FT-IR), Powder X-ray diffraction (PXRD), and surface area determination by BET/BJH. Solubility and bioactivity tests were performed, as well as tests of the bactericidal effect of the synthesized materials using gram-positive *Staphylococcus Epidermis*, and gram-negative *Pseudomonas aeruginosa* strains. The results suggest that the synthesized glasses and scaffolds are bioactive and bactericidal for the strains tested, and their composition favoring the formation of apatite nuclei which helps in the regeneration of bone tissue.

2. Results and Discussion

2.1 Preparation of glass and scaffolds

The glass was obtained by sol-gel method using phosphoric acid as a source of phosphate ions and as a catalyst for the TEOS hydrolysis reaction, since this occurs in the presence of acid medium pH 1.5. The resulting solution was initially translucent and after 4 hours under constant heating and stirring, gel formation was observed. The final material appeared as a solid, powdery, grayish appearance [13-14].

The glass synthesis was carried out maintaining the Ca/P ratio equal to 1.64 in order to favor the formation of hydroxyapatite nuclei in the system [15].

The glass solubility tests, SiHp–Ag, show a mass loss corresponding to 4% of its initial mass, while for the scaffolds, SiHp–Ag–S, (10%, 20%, and 30%) the losses observed were 5%, 10%, and 22% respectively. On average, 7% of the added salt was incorporated into the material.

In the case of SiHp–Ag–C scaffolds (10%, 20%, and 30%) obtained by the polymeric calcination method, the percentage of mass loss observed was 13%, 23%, and 33%, respectively. The formation of pores through the calcination process was more efficient since all the added polymer was removed by the introducing of pores when compared to the salt leaching process. The observed mass loss of approximately 3% can be attributed to the release of volatile residual compounds that were trapped in the glass matrix in the synthesis process. Solubility tests indicate a relationship between the increase in pore quantity and the solubility of the SiHp–Ag–C scaffolds (6%, 7%, and 10%). However, this behavior was not observed for SiHp–Ag–S scaffolds, since this was obtained by the leaching process where salt removal and total mass loss occurred simultaneously.

2.2 Characterization of glass and scaffolds

In the FTIR spectra of the scaffolds, Figure 1, it is possible to observe a set of bands at 3500 to 3200 cm^{-1} and 1600 cm^{-1} that are attributed to asymmetric and symmetric stretching vibrations and angular deformation of hydrogen bond and the hydroxyl group (–OH). The band at 1480-1490 cm^{-1} can be attributed to the asymmetric stretching mode of CO_3^{2-} [16].

The broadband observed in the 1200–930 cm^{-1} range can be attributed to the Si–O–Si stretching vibration. The V_3 and V_1 vibrational modes of the phosphate groups, PO_4^{3-}, also present bands in this region, however considering that they are less intense bands, they overlap the bands of siloxane groups. Bands observed at 940 cm^{-1} refer to the stretching of Si–O–NBO bonds (non-bridged oxygen) [17].

The network modifier ions (PO_4^{3-}, Ag^{+}, and Ca^{2+}) present in the composition of the glasses cause a disturbance in the glass matrix, which generates the occurrence of non-bridge-forming oxygens (NBO). Silica dissolution is controlled through these functional groups that form silanol groups (Si–OH) in the medium [17]. These ions hey are incorporated into the silicate network by ion exchange processes in non-bridged terminal groups, Si–O–H transformed into Si–O–Ag [13] weakening the vitreous network.

The characteristic bands of the Si–O bond appear at 880 cm^{-1} and 1201 cm^{-1}. The weak intensity band between 800–710 cm^{-1} corresponds to Si–O–Si symmetric stretching. Si-O-Si flexion occurs in the 450-490 cm^{-1} range. The greater intensity of the band observed in this region is due to the densification of the vitreous structure due to increased binding. The bands between 620 cm^{-1} and 520 cm^{-1} refer to the V_4 asymmetric and symmetric vibrational modes of PO_4^{3-} and calcium phosphate Ca^{2+}, which reinforces the hypothesis of the presence of this group in the vitreous network [18].

In Figures 2A and 2B are the Powder X-ray diffractograms of the SiHp–Ag standard sample and the SiHp–Ag–S and SiHp–Ag–C scaffolds. The diffraction peaks are characteristic of the structural organization in the region at 2θ = 27.5º and 33.0º, and therefore the presence of crystalline phases can be observed in the SiHp–Ag sample (a) and SiHp-Ag-S scaffolds (Figure 2A: b, c, and d). The X-ray patterns of the glass and scaffold samples show crystallization peaks at 2θ = 27°, 32°, 50°, 54°, 57° corresponding to the planes (002), (112), (321) and (322) respectively, which are attributed to the

hydroxyapatite phase $Ca_5(OH)(PO_4)_3$ present in the material (JCPDS #84-1998) and diffraction peaks at 2θ = 29° corresponding to the silica peak (211) [18]. Also note a diffraction peak at 2θ = 46° and 77° corresponding to planes (220) and (311), indicating the presence of crystallized Ag in a cubic system in the material (JCPDS #04-0783) [19].

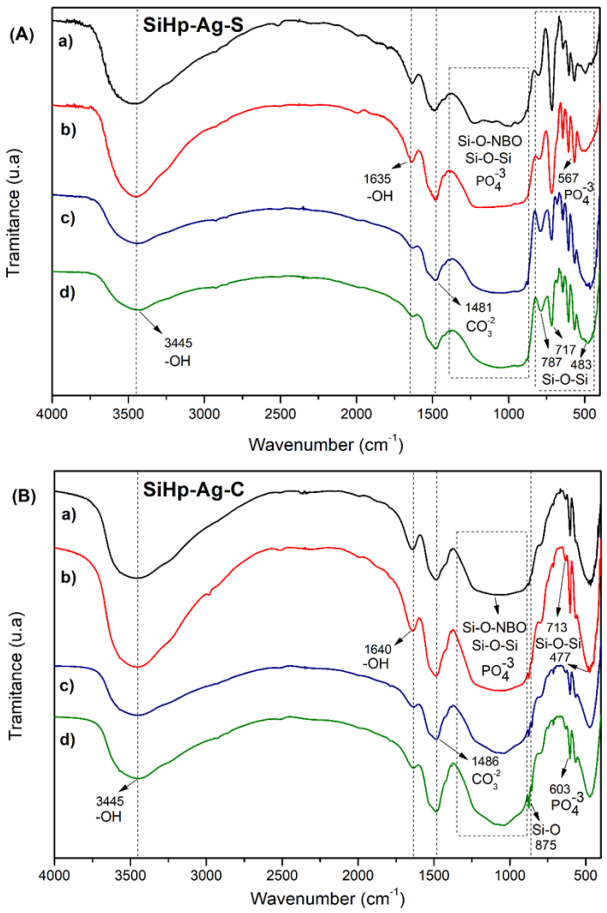

Fig. 1. FTIR vibrational spectra of scaffolds **(A)** SiHp–Ag–S and **(B)** SiHp–Ag–C with a) pure SiHp–Ag, b) 10% pores, c) 20% pores, and d) 30% pores.

Analyzing the 2B SiHp–Ag–C scaffolds of Figure 2B, it can be seen that there is a loss in the degree of crystallinity of the scaffolds. In the calcination process to obtain the scaffolds, it is considered that the complete decomposition of the cellulose formed CO_2 and H_2O. The loss of crystallinity observed in these scaffolds can be attributed to the interaction of the cellulose decomposition product with the structure of the scaffolds, interfering with their crystallinity.

Table 1 shows the results of surface area (SBET), pore volume (Vp) and pore diameter (Dp) obtained from the adsorption-desorption isotherms of the SiHpAg samples (standard glass) and SiHp–Ag-S, SiHp–Ag–S, and SiHp–Ag–C scafollds.

The analyzed materials present type IV isotherms with mesopores and type H1 hysteresis curve that corresponds to cylindrical pores. The addition of silver to the initial glass composition causes a reduction in the specific surface area and an increase in pore diameter. The pore diameter is partially related to the structure of the agents used and not directly to the silica content in the sample [20].

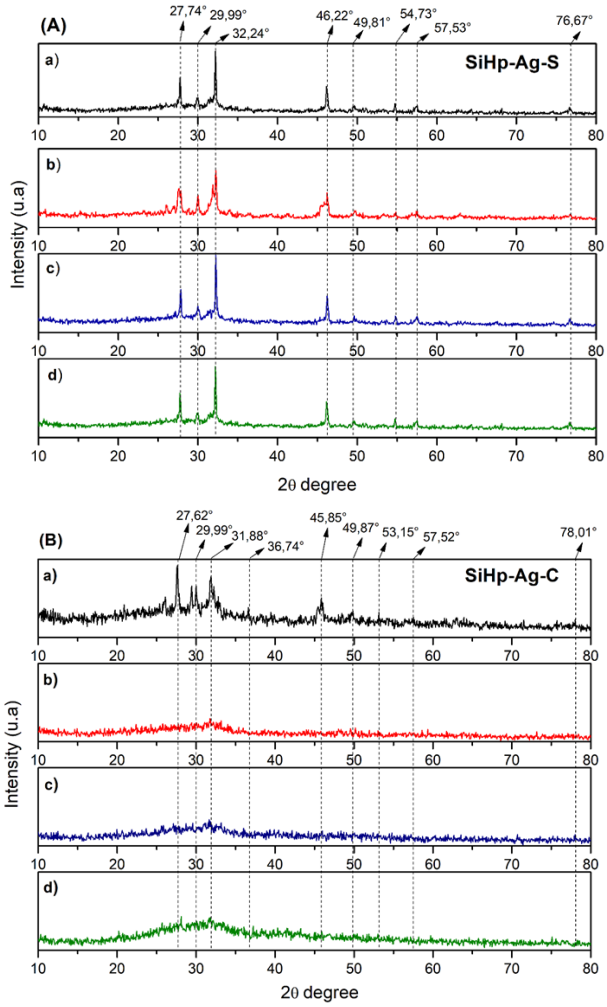

Fig. 2. Powder X-ray diffractograms of the SiHp–Ag pattern (a) and scaffolds **(A)** SiHp–Ag–S and **(B)** b) 10% pores, c) 20% pores, and d) 30% pores.

Table 1. BET-BJH results of SiHp–Ag, SiHp–Ag–S and SiHp–Ag–C samples.

Samples	Surface area ($m^2.g^{-1}$)	Pore volume ($cm^3.g^{-1}$)	Pore size (nm)
SiHp	78.26	0.183	9.331
SiHp–Ag	29.72	0.137	18.49
SiHp–Ag–S	21.72	0.048	1.810
SiHp–Ag–C	13.91	0.032	2.012

2.3 Bioactivity test

An important feature of biomaterials is their bioactivity, which is related to the ability of the material to interact *in vivo* with the host tissue, establishing with it and with body fluids the ion exchange processes that promote tissue restoration. The greater the chemical and structural similarity between the studied material and the host tissue, the greater the interaction between them and the greater the bioactivity of the system. The bioactivity of the SiHp–Ag–S and SiHp–Ag–C scaffolds was observed by placing the samples in the presence of a solution that simulates body fluid (SBF).

The Powder X-ray diffractograms of the scaffolds after contact with the SBF solution are shown in Figure 3. An increase in the degree of crystallinity of the system is observed, mainly for the SiHp–Ag–C scaffolds. Before, Figure 2B, one can see a diffraction halo around 25° corresponding to the amorphous phase of the SiO_2 matrix and weak diffraction peaks in the 2θ region between 27° and 32°

characteristic of phases rich in apatite and hydroxapatite nuclei. After contact with the SBF solution, a more organized structure is noted for the better definition and increased intensity of diffraction peaks located at 2θ = 27°, 30°, 32°, 46°, 54°, and 57°, indicating the growth of phases that corresponding to hydroxyapatite in the scaffolds suggesting a solid/solution interaction [21].

The mechanism of apatite and hydroxyapatite formation occurs when scaffolds are submerged in the SBF solution and the process of ionic exchange, dissolution, and deposition on the surface of the solid is established. In this process, Ca^{2+} ions readily react with H^+ ions in the solution, breaking Si–O–Si bonds in the glass network, increasing the pH of the solution and exposing the silica-rich phase, forming silanol groups. The migration of Ca^{2+} and PO_4^{3-}, which are present in high concentration in the solution to the surface of the solid precipitating as apatite and hydroxyapatites, begins. Si and Ag act as a nucleation center for the formation of apatite, increasing the ionic activity product of apatite [22].

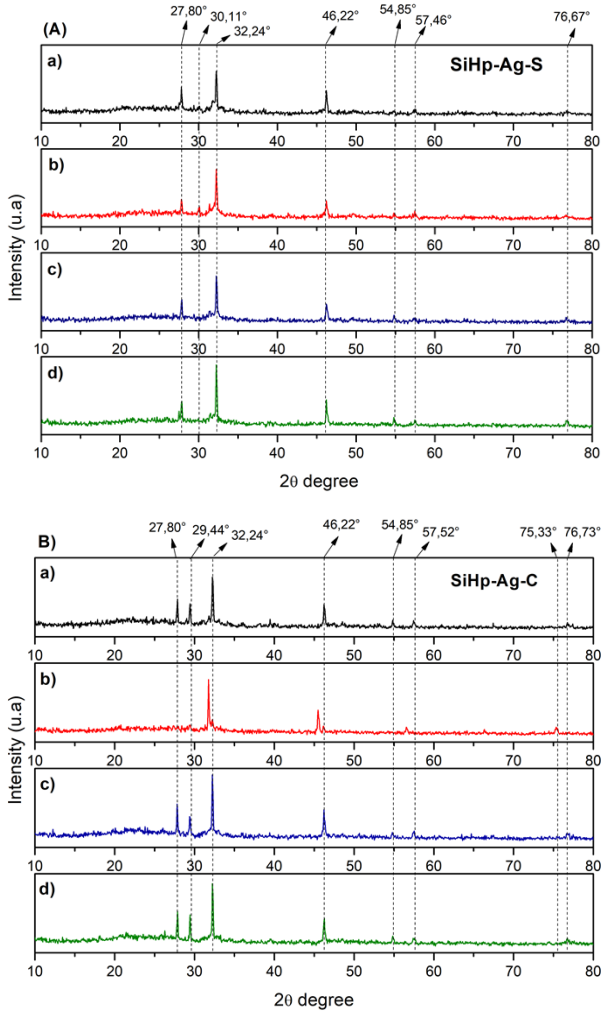

Fig. 3. Powder X-ray diffractograms of scaffolds **(A)** SiHp–Ag–S and **(B)** SiHp–Ag–C with a) pure SiHp–Ag b) 10% pores c) 20% pores, and d) 30% pores after contact with the SBF solution.

Crystallization peaks located at 2θ = 76° present in scaffolds may be associated with the stability of metallic silver nanoparticles that form during the sintering process of scaffolds, becoming trapped in the matrix [14]. Vulpoi and collaborators report that the presence of metallic silver in scaffolds improves or preserves the formation of apatite in bioactive materials [23].

Figure 4 shows the pH variation graphs of the SBF as a function of the scaffolds exposure time. Analyzing the graphs for SiHp–Ag–S and SiHp–Ag–C, one can observed an increase in the initial pH of the SBF solution from 7.3 to approximately 8.2. The increase in the pH of the reaction medium is verified whenever an ionic exchange process is established between solid and solution, indicating the bioactivity of the scaffolds studied [7]. The variation in pH is more pronounced in the first few days followed by a slower increase until equilibrium is reached.

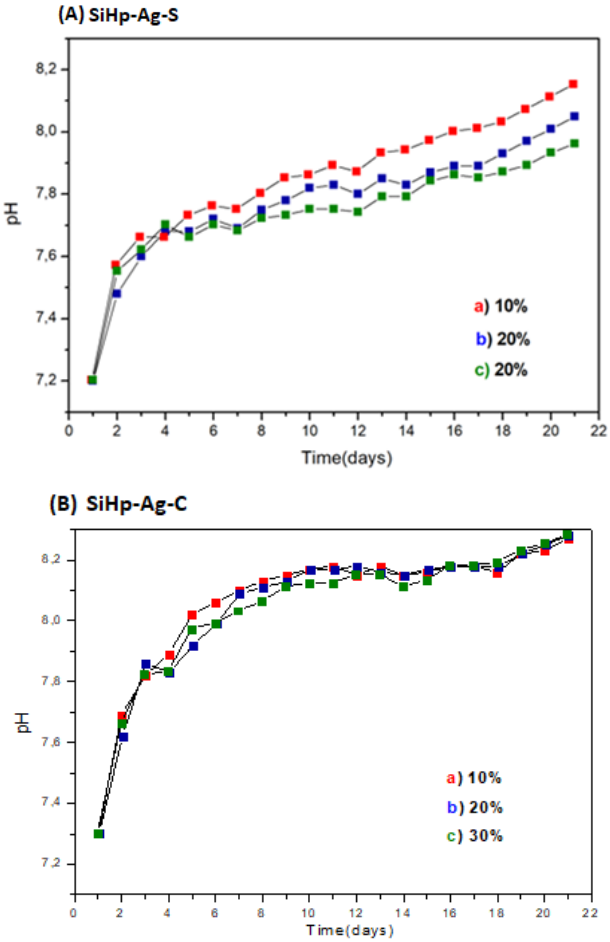

Fig. 4. Influence of scaffolds on pH of the SBF solution as a function of contact time: **(A)** SiHp–Ag-S **(B)** SiHp–Ag–C: a) 10% of pores b) 20% of pores, and c) 30 % of pores.

2.4 Bactericidal activity

Bactericidal tests were initially performed with glass since silver is a known bacterial agent. The results of the bacterial sensitivity tests for the glasses with different concentrations of silver are shown in Table 2. It is observed that the glasses containing silver in different concentrations showed similar or better performance than the antibiotic kanamycin used as a standard for control of the bacterium *Pseudomonas aeruginosa*. For SiHp–Ag-1.0 and SiHp–Ag-2.0 glasses, the inhibitory effect against the strain studied was higher than that of the antibiotic. The bacterium *Pseudomonas aeruginosa* has gram-negative serology and is often associated with infections in orthopedic implants [24].

A proportional increase in the bactericidal activity of the glasses was not observed with the increase in the amount of silver above 1%, therefore, the glass chosen to obtain the scaffolds was SiHp–Ag-1.0.

Inhibition halos of the *Staphylococcus epidermis* strain in the presence of SiHpAg-1.0 glass samples and SiHp–Ag–C and SiHp–Ag–S scaffolds with 10, 20, and 30% pores are shown in Table 3.

Table 2. *Pseudomonas aeruginosa* inhibition halo in the presence of glass samples containing different concentrations of silver.

Inhibition halo (mm): gram-negative *Pseudomonas aeruginosa* strain					
Samples					
Kanamycin	SiHp	SiHp–Ag-0.5	SiHp–Ag-1.0	SiHp–Ag-1.5	SiHp–Ag-2.0
14.0	0.00	14.5	16.0	15.0	16.0

Table 3. *Staphylococcus epidermis* inhibition halos in the presence of SiHp–Ag glass samples, SiHp–Ag–C and SiHp–Ag–S scaffolds.

Inhibition halo (mm): gram-positive *Staphylococcus epidermis* strain							
Samples							
Kanamycin	SiHp–Ag	SiHp–Ag–C			SiHp–Ag–S		
		10	**20**	**30**	**10**	**20**	**30**
23.45	17.59	18.57	18.93	13.77	12.52	11.90	9.180

Observing the results shown in Table 3, it is noted that both the glass with silver and the scaffolds have a bactericidal effect against the *Staphylococcus epidermis* strain, although this is lower than that of the antibiotic used. SiHp–Ag–C scaffolds show a more pronounced bactericidal effect when compared to SiHp–Ag–S scaffolds, and the increase in poro amount decreases the bactericidal activity. The bactericidal activity of the SiHp–Ag–C scaffolds can be attributed to the lower crystallinity of the scaffolds resulting in an increase in the specific surface area, improving the bioactive response of the material and providing a greater amount of silver ions to the medium, increasing the antibacterial effect [17].

3. Material and Methods

3.1. Glass preparation

Initially, a glass of composition $49SiO_2$–$31CaO$–$19P_2O_5$–$1Ag_2O$ (% mole) was synthesized by the sol-gel method. To obtain the glass, two solutions A and B were prepared. Solution A containing 14.29 mL of tetraethoxysilane (TEOS) (Sigma-Aldrich) and 2.880 mL of phosphoric acid (H_3PO_4) (NEON) dissolved in 50 mL of ethyl alcohol (NEON) Solution B containing 0.0399 mol $Ca(NO_3)_2.4H_2O$ (Sigma-Aldrich) and 0.0026 mol $AgNO_3$, solubilized in 50 mL of distilled water and ethyl alcohol, 1:1.

The solution A was maintained under constant stirring and at a controlled temperature of 40 °C. After the first 30 minutes, measure the pH of this solution. Then, the solution B was added slowly over the solution A and the final pH was verified. Stirring and temperature control were maintained until gel formation.

The obtained gel was dried in a muffle oven at a temperature of 120 °C for 5 days. Subsequently, calcined at 600 °C for 3h with a heating rate of 2 °C/min in ambient atmosphere. After this period, the cooled solid was ground and sieved through a 106 µm granulometric sieve. The final material will be represented by SiHp–Ag.

3.2. Preparing the scaffolds

Scaffolds were obtained from a mixture of SiHp–Ag glass with amounts of NaCl (SiHp–Ag–S) corresponding to 0, 10, 20, and 30%. These samples were made in triplicate. The scaffold inserts were made using a cylindrical stainless-steel die with an internal diameter of 13.0 mm and a manual hydraulic uniaxial press with a total pressure of 6T. The same procedure was performed using the SiHp–Ag glass with cellulose (SiHp–Ag–C) adding 0, 10, 20, and 30% by mass of the polymer.

The tablets containing the salt were sintered at 650 °C for 2h with a heating rate of 2 °C/min. After this process, the SiHp–Ag–S pellets were cooled to room temperature, placed in 50 mL of distilled water. and stirred in a thermostated bath at a temperature of 37 °C for 72h to remove the salt and test the solubility of scaffolds. After 72h, the pellets were filtered and dried in an oven for one hour at a temperature of 100 °C and weighed. The SiHp–Ag–C scaffolds were obtained by calcining the pellets at a temperature of 650 °C for two hours. The percentage of mass loss of the samples was calculated.

3.3. Characterization of scaffolds

SiHp–Ag glass and scaffolds samples were characterized using Fourier Transform Infrared Spectroscopy (FTIR) and Powder X-Ray Diffraction (PXRD).

For the Fourier Transform Infrared Spectroscopy (FTIR) analysis, the equipment Zetasizer-Nano-Zn-ZEN3600, Perkin Elmer was used. The samples were prepared in the form of tablets in a mixture of KBr considering 1% (m/m) and the spectra were obtained by scanning in the range of 4000 cm^{-1} to 400 cm^{-1} with an accumulation of 16 scans.

The Powder X-ray diffraction analyses were carried out in a Bruker® DRX-D2 Phaser equipment, with CuKα radiation, with a graphite monogrower, 2θ scanning from 10° to 80°, 0.06 increment and 0.025° step.

The surface area (BET), pore volume (VP), and pore diameter (Dp) of the samples were determined through nitrogen adsorption-desorption isotherms by the Brunauer-Emmett-Teller (BET) and Barrett-Joyner-Halenda (BJH) methods.

3.4. Bioactivity test

The scaffolds were submitted to bioactivity tests in the presence of a solution that simulates the composition of blood plasma (SBF). As described in reference [12].

Subsequently, the SiHp–Ag–S and SiHp–C scaffolds were placed in 50 mL of this solution and stirred in a thermostated bath at 36 °C for 21 days, measuring the pH every 24 h. After this period, the SiHp–Ag–S and SiHp–Ag–C samples were dried in an oven at 100 °C for 3 h. The bioactivity of the scaffolds was evaluated by monitoring the initial pH change of the SBF solution and by PXRD analysis.

3.5. Bactericidal test: disc diffusion method

The antimicrobial susceptibility test was performed using two strains of bacteria [25]. 25 µL of *Pseudomonas aeruginosa* and *Staphylococcus epidermidis* stock solution with 0.5 optical density were applied on the surface of plates containing Luria-Bertani broth (LB) and agar. The positive control contains 20 µg/L of the antibiotic kanamycin. The plates were incubated for approximately 16 h at 37 ± 3 °C in a bacteriological oven. Then, the formation of the inhibition halo of bacterial growth around the disks was analyzed.

4. Conclusions

The SiHp–Ag bioglass was synthesized by sol-gel method and used to obtain scaffolds. The introduction of pores to obtain scaffolds from the cellulose calcination and salt leaching techniques proved to be efficient in obtaining porous structures.

The scaffolds initially characterized by FTIR do not present distinctions from their chemical environments. Powdre X-ray diffractograms indicate that scaffolds obtained from salt leaching are more structurally organized. The crystallinity of SiHp–Ag–C scaffolds after contact with SBF is significantly improved by the growth of hydroxyapatite phases. The variation in the pH of the SBF in the presence of the synthesized scaffolds shows that they present bioactivity.

Bacteriological tests with gram-negative *Staphylococcus epidermis* and gram-positive *Pseudomonas aeruginosa* strains in the presence of glass and scaffolds resulted in a positive inhibitory effect.

All scaffolds developed in this work demonstrate potential for use as bone restoration material given their similarity and propensity to develop phases rich in apatites and hydroxyapatites, in addition to being bactericidal.

Acknowledgments

The authors gratefully acknowledge by CNPq and Araucaria Foundation for scholarship.

Author Contributions

Camila Dias de Oliveira and Gabrieli Andressa de Campos: Scientific initiation scholarship holders and project executors in the synthesis and characterization of the materials. Juliana Cheleski Wiggers: Collaborating Professor who guided the bactericidal tests. Elvio A. de Campos: Collaborating Professor who contributed to the discussions of powder X-ray diffractograms and infrared spectra. Silvia Denofre de Campos: Coordinating Professor responsible for the work.

References and Notes

[1] Williams, D. F. The Williams dictionary of biomaterials, Single Ed., Liverpool University Press, Liverpool., Great Britain, 1999.

[2] Ratner, B. D.; Hoffman, A, S.; Schoen, F. J.; Lemons, J. E. An Introduction to Materials in Medicine. 2rd Academic Press, USA, 2004.

[3] Hoover, S.; Tarafder, S.; Bandyopadhyay, A.; Bose, S. *Mater. Sci. Eng. C.* **2017**, *79*, 763. [Crossref]

[4] Dubnika, A.; Loca, D.; Rudovica, V.; Parekh, M. B.; Berzina-Cimdina, L. *Ceram. Int.* **2017**, *43*, 3698. [Crossref]

[5] Saini, K. R.; Prasad, L.; Bagri, L.; Bajpai, A. K. *Colloids Surfaces B Biointerfaces*, **2019**, *177*, 211. [Crossref]

[6] Marsh, A. C.; Mellott, N. P.; Pajares-Chamorro, N.; Crimp, M.; Wren, A.; Hammer, N. D.; Chatzistavrou, X. *Bioact. Mater.* **2019**, *4*, 215. [Crossref]

[7] Zhang, Y.; Cai, X.; Choi, S. W.; Kim, C.; Wang, L. V. Xia, Y. *Biomaterials* **2010**, *31*, 8651. [Crossref]

[8] Raucci, M. G.; Guarino, V.; Ambrosio, L. *Compos. Sci. Technol.* **2010**, *70*, 1861. [Crossref]

[9] Gao, C.; Liu, T.; Shuai, C.; Peng, S. *Sci. Rep.* **2014, *4*,** 1. [Crossref]

[10] Han, P.; Wu, C.; Chang, J.; Xiao, Y. *Biomaterials* **2012**, *33*, 6370. [Crossref]

[11] Xie, Y.; Lan, X. R.; Bao, R. Y.; Lei, Y.; Cao, Z. Q.; Yang, M. B.; Yang, W.; Wang, Y. B. *Mater. Sci. Eng. C*. **2018,** *90*, 602. [Crossref]

[12] Du, Z.; Zhao, Z.; Liu, H.; Liu, X.; Zhang, X.; Huang, Y.; Leng, H.; Cai, Q. Yang, X. *Mater. Sci. Eng. C.* **2020,** *113*, 1. [Crossref]

[13] Jeon, H. J.; Yi, S. C.; Oh, S. G. *Biomaterials* **2003**, *24*, 4921. [Crossref]

[14] Scalera, F.; Gervaso, F.; Sanosh, K. P.; Sannino, A.; Licciulli, A. *Ceram. Int*. **2013**, *39*, 4839. [Crossref]

[15] Kourkoumelis, N.; Balatsoukas, I.; Tzaphlidou, M. *J. Biol. Phys.* **2012**, *38*, 279. [Crossref]

[16] Zheng, K.; Balasubramanian, P.; Paterson, T. E.; Stein, R.; MacNeil, S.; Fiorilli, S.; Vitale-Brovarone, C.; Shepherd, J.; Boccaccini, A. R. *Mater. Sci. Eng. C*. **2019**, *103*, 1. [Crossref]

[17] Khan, M. U. A.; Abd Razak, S. I.; Mehboob, H.; Abdul Kadir, M. R.; Anand, T. J. S.; Inam, F.; Shah, S. A.; Abdel-Haliem, M. E. F.; Amin, R. *ACS Omega* **2021**, *6*, 4335. [Crossref]

[18] Najafizadeh, F.; Sadjadi, M. A. S.; Fateami, S. J.; Mobarakeh, M. K.; Afshar, R. M. *Orient. J. Chem.* **2016**, *32*, 1639. [Crossref]

[19] Shuai, C.; Xu, Y.; Feng, P.; Wang, G.; Xiong, S.; Peng, S. *Chem. Eng. J.* **2019**, *374*, 304. [Crossref]

[20] Atkinson, I.; Anghel, E. M.; Predoana, L.; Mocioiu, O. C.; Jecu, L.; Raut, I.; Munteanu, C.; Culita, D.; Zaharescu, M. *Ceramic International* **2016**, *42*, 3033. [Crossref]

[21] Kokubo, T.; Takadama, H. *Biomaterials* **2006**, *27*, 2907. [Crossref]

[22] Jones, J. R. *Acta Biomaterialia* **2013**, *9*, 4457. [Crossref]

[23] Vulpoi, A.; Gruian, C.; Vanea, E.; Baia, L.; Simon, S.; Steinhoff, H. J.; Göller, G.; Simon, V. *J. Biomed. Mater. Res.-Part A* **2012**, *100A*, 1179. [Crossref]

[24] Cerioli, M.; Batailler, C.; Conrad, A.; Roux, S.; Perpoint, T.; Becker, A.; Triffault-Fillit, C.; Lustig, S.; Fessy, M-H.; Laurent, F.; Valour, F.; Chidiac, C.; Ferry, T. *Frontiers in Medicine*, **2020,**1. [Crossref]

[25] Available from: **http://www.anvisa.gov.br/servicosaude/manuais/clsi/clsi_opasm2-a8.pdf.** Access February 2020.

How to cite this article

de Oliveira, C. d.; de Campos, G. A.; Wiggers, J. C.; de Campos, E. A.; de Campos, S. D. *Orbital: Electronic J. Chem*. **2025**, *17*, 179. DOI: **http://dx.doi.org/10.17807/orbital.v17i2.20255**